ELSEVIER

Journal of Crystal Growth 222 (2001) 380–391

JOURNAL OF CRYSTAL GROWTH

www.elsevier.nl/locate/jcrysgro

Measurement of the density of succinonitrile–acetone alloys

D.L. Ceynar, C. Beckermann*

Department of Mechanical Engineering, The University of Iowa, 2212 Engineering Building, Iowa City, IA 52242, USA

Received 8 June 2000; accepted 30 September 2000
Communicated by M.E. Glicksman

Abstract

Measurements are reported of the liquid and liquid–solid mixture (mush) densities of succinonitrile–acetone (SCN–ACE) alloys for use in crystal growth and solidification studies. The measured data for the liquid is analyzed and consolidated into a correlation that expresses the liquid density as a function of composition and temperature. This correlation also allows for the calculation of the thermal and solutal coefficients of volume expansion for liquid SCN–ACE alloys. Using the measured results for the liquid–solid mixture densities, the solid densities of SCN–ACE alloys during solidification in a mushy mode are estimated based on either the Lever or Scheil solidification model, and are found to be close to solid densities for pure SCN.

PACS: 06.30.Dr; 81.30.Fb; 65.70.+y

Keywords: Density; Solidification; Succinonitrile; Acetone; Alloy; Mush

1. Introduction

Succinonitrile–acetone (SCN–ACE) is a transparent alloy widely used as a model material for crystal growth and solidification studies [1–7]. It has low entropy of fusion, weak anisotropy of surface tension, and rapid molecular attachment kinetics, all of which are analogous to the corresponding properties of metal alloy systems. The optical transparency and low melting temperatures ($<58^{\circ}C$) of this alloy permit experimentally convenient in situ observation of the growth rates, solidification structures, and melt flow patterns; a task that is difficult for opaque metal systems. These attributes make the SCN–ACE alloy extremely valuable for experimental investigations of solidification processes.

For use as a model material in solidification studies, the physical properties of the SCN–ACE alloy must be known in order to allow for quantitative comparisons with theories. The mass diffusivity, liquidus slope, and equilibrium partition ratio have been measured for the SCN–ACE alloy [1,2]. Other properties have often been estimated using the well-established values for pure SCN [3,8–10]. For a dilute alloy, such estimates may be reasonable. However, if the

*Corresponding author. Tel.: +1-319-335-5681; fax: +1-319-335-5669.
E-mail address: becker@engineering.uiowa.edu (C. Becker-mann).

0022-0248/01/$ - see front matter
PII: S0022-0248(00)00905-2

interest is in more concentrated alloys or in the effect of solute additions on the solidification process, the dependence of the properties on the solute concentration must be precisely assessed. This is especially important for the liquid and solid densities during solidification of alloys when investigating the influence of thermo-solutal natural convection of the melt; the settling of unattached solid, such as small equiaxed grains or dendrite fragments in the melt; solidification shrinkage-driven flow; hot tears inside a mushy zone; or porosity formation. Unfortunately, the densities of SCN-ACE alloys have not been measured as a function of temperature and solute concentration. In general, direct measurements of the densities of alloys during solidification are extremely rare. In particular, solid densities in the solidification temperature range are often extrapolated from measurements of the density of fully solid samples below the solidus temperature. This practice is questionable because of the presence of microsegregation and secondary phases (e.g., the eutectic) in fully solid alloys.

This paper presents experimental measurements of the density of SCN–ACE alloys relevant to crystal growth and solidification studies. Using a flask that was designed to provide highly accurate measurements of volume, liquid and liquid–solid mixture densities were determined as a function of temperature for alloy concentrations up to $\sim$18 wt% ACE. In the following, the term 'liquid–solid mixture' refers to a mush consisting of dendritic solid finely dispersed in the liquid. The results for the liquid are consolidated by regression analysis into a composite correlation, which can also be used to calculate the thermal and solutal expansion coefficients of liquid SCN–ACE alloys as a function of temperature and composition. Using the measured liquid–solid mixture densities and solid fraction estimates from either the Lever Rule or Scheil's equation, the variation of the solid density during solidification of several SCN–ACE alloys was determined. In addition, the solid density of 99.7% pure SCN at room temperature was measured using a separate procedure. The results in the limit of vanishing ACE concentration are compared with various density data for pure SCN found in the literature.

2. Experimental setup and procedures

The density of the SCN–ACE alloy was determined by measuring the mass and volume of a sample at a given temperature and com-position, and atmospheric pressure. The mass measurements were performed using an electronic balance with an accuracy of 0.4 mg. The volume measurements, and the resulting density determination, are described in the next section. The temperature and solute concentration measurements, as well as other experimental procedures and an uncertainty analysis, are presented in subsequent subsections.

2.1. Flask design and calibration

The volume measurements were performed using the specially designed volumetric flask shown in Fig. 1. The flask was constructed of a $\sim$58 cm^3 borosilicate glass bulb and a 4 mm (inner diameter) capillary tube, which were joined by the glass blower with a small amount of uranium glass in order to accommodate any differential thermal expansion. The capillary tube was pre-marked with 1/100 cm^3 graduations at 20°C. The geometry of the flask was chosen such that a relatively small volume change results in a large change in the meniscus position in the capillary tube.

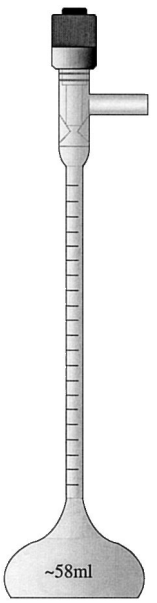

Fig. 1. Density measurement flask.

The initially unknown volume of the flask, corresponding to one of the graduations on the capillary tube, was determined using the methodology described in an ASTM Standard for the calibration of volumetric flasks [11]. This standard chooses distilled water as a calibration material and 20°C as the standard calibration temperature. The concept of the calibration is simple: knowing the density of water, ρ_w, at the temperature T [12] and measuring the mass of the water contained in the flask, M_w, the volume of the flask at T, V_T, can be calculated from $V_T = M_w/\rho_w$. However, this expression cannot be used directly, because of the presence of buoyancy and thermal expansion of the glass. Taking those effects into account, the volume at the standard calibration temperature of 20°C is given by

$$V_{20} = \frac{M_L - M_E}{\rho_w - \rho_a}[1 - \alpha(T - 20)] \quad (1)$$

where M_L is the balance indication of the loaded (filled) flask in grams, M_E is the balance indication of the empty (air filled) flask in grams, ρ_a is the density of the air in the flask in g/cm^3, α is the coefficient of thermal expansion of the flask in °C^{-1}, and T is the temperature of the flask in °C. The coefficient of thermal expansion of the flask was measured as part of the present study. It was found to be $\alpha = 2.5 \times 10^{-5}$ °C^{-1}, which is in agreement with literature values for the type of glass used. Using distilled water, it was verified that α varies by less than 0.1×10^{-5} °C^{-1} over a temperature range from 15°C to 50°C. Temperatures were measured using calibrated thermocouples with an accuracy of ± 0.1°C.

Using the calibrated flask to measure the volume, V, the density of the SCN–ACE alloy, ρ, at any temperature can then be determined from

$$\rho = \frac{(M_L - M_E)[1 - \alpha(T - 20)]}{V} + \rho_a \quad (2)$$

2.2. Preparation of the SCN–ACE alloy and determination of concentration

The succinonitrile and acetone used to prepare the SCN–ACE alloy were as-received 99% and 99.7% pure, respectively. The two substances were mixed in a sealed flask at a temperature approximately 20°C above the liquidus temperature.

The concentration of acetone in the SCN–ACE alloy, C_o, was determined by measuring the liquidus temperature, T_L. For the present range of concentrations, the liquidus line in the SCN–ACE equilibrium phase diagram is accurately represented by a linear relationship [1,2], such that

$$C_o = (T_L - T_0)/m \quad (3)$$

where T_0 is the melting temperature of pure SCN and m is the liquidus slope. The values $T_0 = 58.081$°C and $m = -2.8 \pm 0.08$ K/wt% [1,2] were used throughout the present study. The uncertainty in the liquidus slope was estimated from the plots in Refs. [1,2].

The liquidus temperature was measured according to the following procedure. The flask containing the SCN–ACE alloy was submerged in a large, temperature-controlled bath, completely melted, thoroughly stirred, and then cooled below the liquidus temperature to nucleate small crystals. Next the temperature of the bath was slowly increased every 30 min, in increments of 1°C, to melt the crystals. When the temperature approached T_L and the crystals became very small, the increments were adjusted to 0.1°C/h. The long hold times, together with repeated stirring, allowed the solid–liquid mixture to reach equilibrium. Since thermal equilibrium is attained quickly, diffusion of solute in the liquid is the rate-limiting process for reaching equilibrium. Considering the slow melting rates (less than 1 μm/s), the small size of the crystals (less than 1 mm), and the mass diffusivity of ACE in SCN (1.3×10^{-9} m^2/s), the characteristic solute diffusion time is less than 1000 s. The temperature at which the last crystal melted was taken as the liquidus temperature, T_L. Combining the uncertainties in the temperature measurement (± 0.1°C) and the crystal melting observation (± 0.1°C) yields an overall uncertainty of ± 0.14°C in T_L. Repeated measurements, using different stirring procedures and even longer hold times, verified this uncertainty in the measured liquidus temperature. Together with the estimated uncertainty in the liquidus slope m (± 0.08 K/wt%), the corresponding uncertainty in the acetone concentration ranges from 0.15

wt% for $C_o = 4.9$ wt% to 0.52 wt% for $C_o = 17.7$ wt% (i.e., about 3% of C_o).

It should be noted that for the alloys prepared from the as-received impure SCN and ACE, a concentration calculated from Eq. (3) actually represents an equivalent acetone concentration which includes the effect of the impurities on the liquidus temperature. The as-received SCN was found to have a liquidus temperature of 56.7°C, which is about 1.4°C below the melting point of pure SCN. Hence, the impurities in the SCN are equivalent to 0.5 wt% ACE. Because most of the present density measurements are carried out at much higher ACE concentrations, the effect of the impurities is small. More importantly, as is shown below, the extrapolation of the present density measurements to vanishing solute concentrations gives liquid densities that are in excellent agreement with literature data for very pure SCN.

2.3. Experimental procedure

Before use, the volumetric flask was thoroughly cleaned with several successive rinses of distilled water and ACE, dried with a heat gun, and weighed to obtain its empty mass. The flask was then filled with the SCN–ACE alloy and weighed again to determine its loaded mass. The loaded flask was immersed in a large, temperature-controlled water bath capable of maintaining a temperature uniformity of ±0.05°C to perform the liquidus temperature and volume measurements. The liquidus temperature was measured before and after each experiment and found to be the same within the stated uncertainty.

The variation in volume of the SCN–ACE alloy with temperature was measured by incrementally decreasing the temperature of the bath and noting the respective volume reading on the flask at each temperature. Here, care was taken to determine the position of the meniscus in the capillary tube in a manner consistent with the volume calibration. The measurements were started at a temperature approximately 20–30°C above T_L, and ended at a temperature below T_L when the solid fraction was no more than 30% (as estimated from the Lever Rule; see below). Hence, densities were measured in both the single-phase liquid and the liquid–solid mixture region of the SCN–ACE phase diagram. The solid consisted of dendrites finely dispersed in the liquid (i.e., a mush). The flask was held at each temperature for at least 30 min, with periodic shaking and mixing of the solution. The measurements were terminated at a solid fraction of no more than 30%, because at higher solid fractions mixing of the solid–liquid mixture becomes ineffective and reading of the meniscus position is unreliable.

2.4. Uncertainty analysis

In view of Eq. (2), the uncertainty in the density measurement, $\delta\rho$, arises from errors in the measured masses, M_L and M_E, volume, V, thermal expansion coefficient, α, and temperature, T. Errors in the air density, ρ_a, are negligible. Hence, the uncertainty can be estimated from

$$\delta\rho = \left[\left(\frac{\partial\rho}{\partial M_L}\delta M_L\right)^2 + \left(\frac{\partial\rho}{\partial M_E}\delta M_E\right)^2 + \left(\frac{\partial\rho}{\partial\alpha}\delta\alpha\right)^2 + \left(\frac{\partial\rho}{\partial T}\delta T\right)^2 + \left(\frac{\partial\rho}{\partial V}\delta V\right)^2\right]^{1/2} \quad (4)$$

where the partial derivatives are obtained from Eq. (2). The estimated uncertainties in the measured quantities are $\delta M_L = \delta M_E = 0.4 \times 10^{-3}$ g, $\delta\alpha = 0.1 \times 10^{-5}{}^{o}\mathrm{C}^{-1}$, $\delta T = 0.1$°C, and $\delta V = 7.6 \times 10^{-3}$ cm^3. The resulting uncertainty in each single density measurement is $\delta\rho = 1.4 \times 10^{-4}$ g/cm^3, which can be considered very low. Virtually all of the uncertainty arises from the volume measurement and is related to identifying the meniscus position in the capillary tube. Although a smaller inner diameter of the capillary tube would reduce the uncertainty of the volume measurement for the liquid, it prevents effective stirring of the solid–liquid mixture for the density measurements below the liquidus temperature. Thus, the chosen inner diameter of 4 mm represents a compromise between accuracy and the ability to perform density measurements for a homogeneous solid–liquid mixture.

3. Results and discussion

Fig. 2 shows the results of the density measurements as a function of temperature at various alloy concentrations, C_o. Based on these results, a correlation for the liquid density was derived, the thermal and solutal expansion coefficients of the liquid were determined, the liquid–solid mixture density was correlated, and the solid density was estimated. The details are discussed in the following subsections.

3.1. Correlation for liquid density

A correlation for the density of liquid SCN–ACE alloys as a function of temperature and solute concentration can be derived from the density measurements above the liquidus temperature, T_L. It can be seen from Fig. 2 that the measured liquid density at a given alloy concentration, C_o, shows excellent linearity with temperature, i.e. $\rho_l = a_l T + b_l$. The values of the coefficients a_l and b_l, obtained by linear regression analysis of the liquid densities measured at each concentration, are summarized in Table 1. The 95% confidence intervals (CI) between the measured densities and the linear fits at each C_o shown in Table 1 are well within the stated uncertainty in the density measurement. Figs. 3 and 4 show that the variation of the coefficients a_l and b_l with concentration can be closely described by the following curve fits:

$$a_l = -3.04 \times 10^{-6} C - 7.810 \times 10^{-4} \quad (5a)$$

$$b_l = -1.40 \times 10^{-5} C^2 - 2.114 \times 10^{-3} C + 1.0334 \quad (5b)$$

where C is the concentration of ACE in the liquid in wt%, a_l is in g/(cm^3 K), and b_l is in g/cm^3.

Substituting Eqs. (5a and 5b) into the expression $\rho_l = a_l T + b_l$, yields the following composite correlation for the liquid density of SCN–ACE alloys

$$\rho_l = [(-3.04 \times 10^{-6} C) - 7.810 \times 10^{-4}] T + (-1.40 \times 10^{-5} C^2) - (2.114 \times 10^{-3} C) + 1.0334 \quad (6)$$

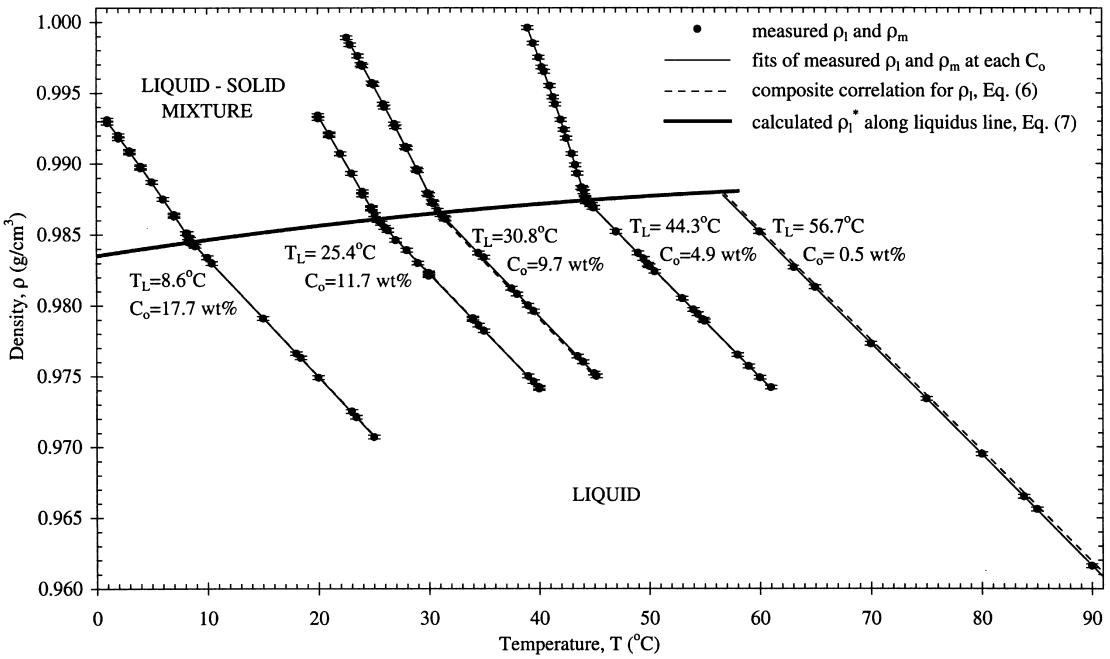

Fig. 2. Liquid and liquid–solid mixture densities of SCN–ACE versus temperature for various alloy concentrations.

Table 1
Results of linear regression analysis of measured liquid densities, $\rho_l = a_l T + b_l$ (g/cm^3), at various alloy concentrations

T_L (°C)	C_o (wt%)	a_l (g/cm^3/K)	b_l (g/cm^3)	R^2	95% CI (g/cm^3)
56.7	0.5	-7.849×10^{-4}	1.0323	1.0000	8.4×10^{-5}
44.3	4.9	-7.957×10^{-4}	1.0227	0.9999	1.0×10^{-5}
30.8	9.7	-8.109×10^{-4}	1.0117	0.9999	1.03×10^{-4}
25.4	11.7	-8.099×10^{-4}	1.0065	0.9998	1.24×10^{-4}
8.6	17.7	-8.391×10^{-4}	0.9917	0.9999	9.7×10^{-5}

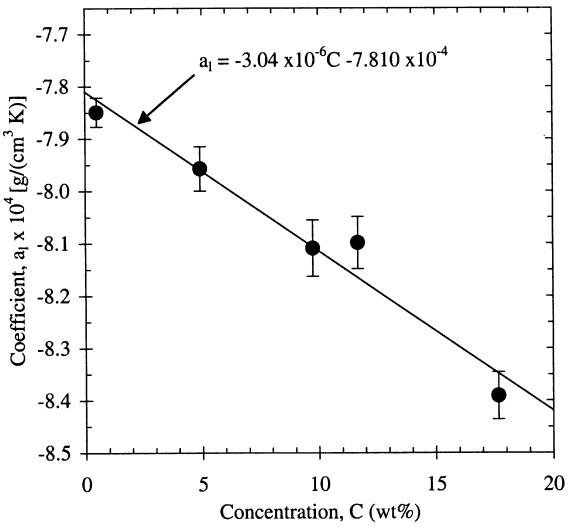

Fig. 3. Variation of the coefficient a_l with concentration; the symbols represent the results from the regression analysis of measured liquid densities; the error bars represent the 95% CI from regression analysis of the measured data at each alloy concentration.

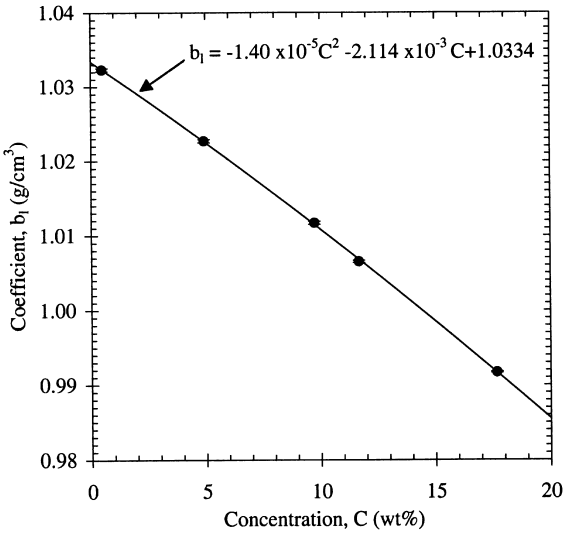

Fig. 4. Variation of the coefficient b_l with concentration; the symbols represent the results from the regression analysis of measured liquid densities; the error bars represent the 95% CI from regression analysis of the measured data at each alloy concentration.

where ρ_l is in g/cm^3, C is in wt%, and T is in °C. This composite correlation describes the variation of the liquid density of SCN–ACE alloys with temperature and composition, and is valid for ACE concentrations ranging from 0 to 18 wt% and temperatures ranging from the liquidus temperature to at least 30°C above liquidus. The 95% confidence interval between the correlation and all measured liquid density data is 1.67×10^{-4} g/cm^3, which is close to the measurement uncertainty (1.4×10^{-4} g/cm^3). Therefore, no attempt was made to include higher-order terms in the correlation.

The composite liquid density correlation, Eq. (6), is plotted as dashed lines in Fig. 2 for each of the concentrations measured in the experiments ($C_o = 0.5$, 4.9, 9.7, 11.7, 17.7 wt%). It can be seen that the correlation agrees very well with the measured densities. The largest difference, although still within the confidence interval, exists for $C_o = 0.5$ wt%, which can perhaps be attributed to the effect of the impurities. Excluding those data would not have resulted in significant changes in the coefficients of the liquid density correlation. Using Eq. (6), the liquid densities of pure SCN ($C = 0$) at various temperatures are calculated and compared with literature values in Table 2. The calculated densities are found to be in excellent agreement with the reported data for pure liquid SCN [13–16].

The liquid density correlation, Eq. (6), can also be used to calculate the density of a saturated SCN–ACE solution, ρ_l^*. If it can be assumed that the liquid is well mixed and in equilibrium with the solid (as is usually the case for the interdendritic liquid in a mushy zone), ρ_l^* can be taken as the density of the liquid inside the mushy zone during solidification of SCN–ACE alloys. Substituting the relation for the liquidus line, $C = (T - T_0)/m$, for the concentrations in Eq. (6) yields

$$\rho_l^* = -7.04 \times 10^{-7} T^2 + 1.187 \times 10^{-4} T + 0.98352 \quad (7)$$

where ρ_l^* is in g/cm^3 and T is in °C. This result is also plotted in Fig. 2. It can be seen that the density of the saturated liquid changes by less than 0.5% over the entire 60°C temperature range plotted in Fig. 2. As the temperature of the saturated SCN–ACE solution decreases, the concentration of ACE increases along the liquidus line. These two effects have opposite influences on the liquid density, resulting in the approximate constancy of ρ_l^*.

3.2. Liquid thermal and solutal expansion coefficients

The liquid thermal and solutal expansion coefficients of SCN–ACE alloys can be derived from the liquid density correlation, Eq. (6), using the following definitions:

$$\beta_T = -\frac{1}{\rho_l}\frac{\partial \rho_l}{\partial T} = (a_l T + b_l)^{-1}(3.04\times10^{-6} C + 7.810\times10^{-4}) \quad (8)$$

$$\beta_C = -\frac{1}{\rho_l}\frac{\partial \rho_l}{\partial C} = (a_l T + b_l)^{-1}(3.04\times10^{-6} T + 2.81\times10^{-5} C + 2.114\times10^{-3}) \quad (9)$$

where β_T is in K^{-1}, β_C is in wt%$^{-1}$, C is in wt%, and T is in °C. The above equations are shown in Figs. 5 and 6 as plots of β_T and β_C, respectively, versus concentration, C, at various temperatures.

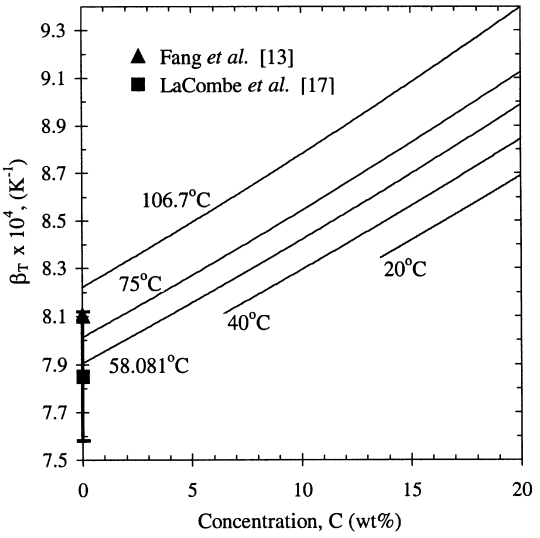

Fig. 5. Variation of the thermal volumetric expansion coefficient β_T, with concentration at various temperatures.

It can be seen that both β_T and β_C increase with temperature and concentration.

Using Eq. (8), β_T was calculated for pure SCN ($C = 0$) at the melting temperature, $T_m = 58.081$°C, and compared with other experimental results from the literature. The calculated value, 7.91×10^{-4} K^{-1}, is in good agreement with the value $7.85 \times 10^{-4} \pm 0.27 \times 10^{-4}$ K^{-1} obtained by LaCombe et al. [17] for 99.99% pure SCN. It also compares well with the value of 8.1×10^{-4} K^{-1}, reported by Fang et al. [13]. It should be noted that LaCombe et al. measured the thermal expansion coefficient directly (i.e., without determining densities first) over a temperature range from 67.3 to 106.7°C, based on the assumption that β_T is temperature independent. This means their value reflects an average thermal expansion coefficient of pure SCN over that temperature range. In fact, the excellent linearity of the liquid density with temperature found in the present study (see Table 1) implies, according to Eq. (8), that β_T is temperature dependent. However, as can be seen from Fig. 5, this dependency is relatively weak. Using Eq. (8), β_T of pure SCN increases from 7.96×10^{-4} K^{-1} at 67.3°C to 8.22×10^{-4} K^{-1} at 106.7°C. This increase of about

Table 2
Comparison of liquid densities of pure SCN calculated from Eq. (6) with data available in the literature; the densities from the International Critical Tables are obtained from a given linear correlation; no uncertainties are available for the data of Refs. [13,15,16]

T (°C)	Present correlation, Eq. (6) ρ_l (g/cm^3)	Int. Critical Tables [14] $\rho_l \pm 0.2\times10^{-2}$ (g/cm^3)	Other data ρ_l (g/cm^3)
58.081	0.9880	0.9895	0.988 [13]
63.1	0.9841	0.9855	0.9848 [15]
75.0	0.9748	0.9760	
83.8	0.9680	0.9690	0.9686 [16]
90.0	0.9631	0.9640	

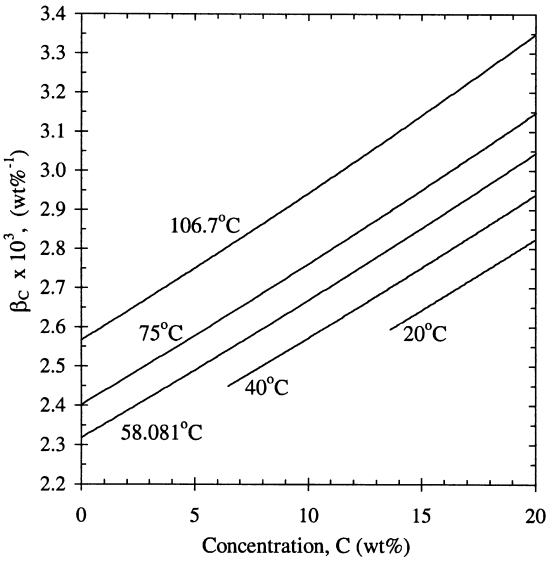

Fig. 6. Variation of the solutal expansion coefficient, β_C, with concentration at various temperatures.

3% is roughly equivalent to the measurement uncertainty reported by LaCombe et al.

3.3. Densities of solid during solidification

The measured densities of the liquid–solid mixture are correlated and used in this subsection to estimate the variation of the solid density during solidification.

3.3.1. Correlation of measured liquid–solid mixture densities

The mixture densities, ρ_m, are shown in Fig. 2 as a function of temperature for each of the alloy concentrations, C_o. It can be seen that the mixture density increases more steeply with decreasing temperature than the liquid density, which can be attributed to the formation of the denser solid. The volumetric solidification shrinkage for pure SCN is approximately 2.8%. For each C_o, the measured mixture densities were fit by a second-order polynomial, $\rho_m = a_m T^2 + b_m T + c_m$, where the coefficients are provided in Table 3. As evidenced by the correlation coefficients and confidence intervals in Table 3, as well as by the lines in Fig. 2, excellent fits are obtained (note: a linear fit was not satisfactory). At the liquidus temperature, T_L, the mixture density, ρ_m, should be equal to the saturated liquid density, ρ_l^*. It can be verified from Eq. (7) and Table 3 that $\rho_m = \rho_l^*$ at T_L to within 0.8×10^{-4} g/cm^3, which is less than the uncertainty in the present density measurements.

3.3.2. Procedure for calculating the solid density

The variation of the solid density, ρ_s, during solidification is calculated based on the following procedure, which is applicable to the finely dispersed liquid–solid mixture (mush) of the present experiment. In the volumetric flask, mass and species are conserved according to, respectively

$$\rho_m = f_s^V \rho_s + (1 - f_s^V)\rho_l \tag{10}$$

$$C_o = f_s^M C_s + (1 - f_s^M) C_l \tag{11}$$

where C_s and C_l are the average solute concentrations in the solid and liquid, respectively, f_s^V is the solid volume fraction, and f_s^M is the solid mass fraction. The two solid fractions are related by

Table 3
Results of polynomial line fit of measured liquid–solid mixture densities, $\rho_m = a_m T^2 + b_m T + c_m$ (g/cm^3), at various alloy concentrations

T_L (°C)	C_o (wt%)	a_m (g/cm^3/K^2)	b_m (g/cm^3/K)	c_m (g/cm^3)	R^2	95% CI (g/cm^3)
44.3	4.9	-6.33×10^{-5}	2.9650×10^{-3}	0.98018	0.9997	8.1×10^{-5}
30.8	9.7	-1.79×10^{-5}	-0.5435×10^{-3}	1.0203	0.9997	8.3×10^{-5}
25.4	11.7	-0.64×10^{-5}	-1.0769×10^{-3}	1.0175	0.9994	9.8×10^{-5}
8.6	17.7	-1.11×10^{-5}	-1.0137×10^{-3}	0.99400	0.9994	8.3×10^{-5}

$$f_s^V = \frac{f_s^M}{(1-f_s^M)\dfrac{\rho_s}{\rho_l} + f_s^M}. \tag{12}$$

Note that the concentrations in the solid and liquid, C_s and C_l, vary during solidification, while C_o is constant. Due to the finely dispersed nature of the solid in the flask, the inter-dendritic liquid can be safely assumed to be well mixed, such that C_l is given as a function of temperature by the liquidus line, i.e. $C_l = (T-T_0)/m$. The liquid density during solidification is then given by Eq. (7), i.e. $\rho_l = \rho_l^*$. Because of slow diffusion of the solute in the dendritic solid during solidification, microscopic variations of the concentration in the solid may be present. Therefore, both C_s and ρ_s should be regarded as average values for the flask. For the two limiting cases of infinitely fast and slow solute diffusion in the solid, the solid mass fraction can be calculated as a function of temperature from either the Lever Rule or the Scheil equation, which are given, respectively, by

$$f_{s-\mathrm{Lever}}^M = \frac{T - T_L}{(1-k)(T-T_0)} \tag{13}$$

$$f_{s-\mathrm{Scheil}}^M = 1 - \left(\frac{T-T_0}{T_L-T_0}\right)^{1/(k-1)} \tag{14}$$

where k is the partition ratio from the SCN–ACE equilibrium phase diagram, taken to be equal to 0.1 wt%/wt% [1,2]. The actual solid mass fraction can be expected to lie between the values given by Eqs. (13) and (14). For the present value of the partition ratio and the low solid fractions present in the experiments ($<30\%$), it can be easily verified that the difference between the two solid fraction estimates is small compared to the uncertainty in the solid fraction itself (see below).

Substituting Eq. (12) into Eq. (10), and taking $\rho_l = \rho_l^*$, yields

$$\rho_s = \frac{f_s^M \rho_m \rho_l^*}{\rho_l^* - (1-f_s^M)\rho_m}. \tag{15}$$

Eq. (15) allows for the calculation of the (average) solid density during solidification from the measured liquid and liquid–solid mixture densities and the solid mass fraction estimates from either Eq. (13) or Eq. (14). At a given temperature, the corresponding (average) ACE concentration in the solid, C_s, can then be obtained from Eq. (11). Again, it can be verified that the use of either Eq. (13) or Eq. (14) causes only minor differences in C_s for the present ranges of the parameters (less than 0.15 wt%).

3.3.3. Uncertainty analysis

In view of Eq. (15), the uncertainty in ρ_s is given by

$$\delta\rho_s = \sqrt{\left(\frac{\partial\rho_s}{\partial\rho_l^*}\delta\rho_l^*\right)^2 + \left(\frac{\partial\rho_s}{\partial\rho_m}\delta\rho_m\right)^2 + \left(\frac{\partial\rho_s}{\partial f_s^M}\delta f_s^M\right)^2} \tag{16}$$

where $\delta\rho_l^*$, $\delta\rho_m$, δf_s^M, are the individual uncertainties in ρ_l*, ρ_m, and f_s^M, respectively. As before, $\delta\rho_l^* = \delta\rho_m = 1.4\times10^{-4}$ g/cm^3. The uncertainty in the solid fraction, δf_s^M, was evaluated from Eqs. (13) or (14) by considering the individual uncertainties in the measured temperatures and phase diagram parameters. The uncertainty was found to increase strongly with decreasing alloy concentration and decreasing solid fraction. For $C_o = 17.7$ wt%, $\delta f_s^M/f_s$

increases from about 3% to 8% as the solid fraction decreases from 15% to 5%. For $C_o = 4.9$ wt%, $\delta f_s^M / f_s$ increases from about 7% to 28% as the solid fraction decreases from 30% to 5%. Only at the highest solid fractions is the uncertainty in f_s^M comparable to the difference caused by the Lever Rule and Scheil equation. The relatively large uncertainties in f_s^M at the lowest alloy concentration are caused by both the steep increase in the solid fraction with decreasing temperature and the uncertainty in the phase diagram parameters.

Differentiating Eq. (15), it can be seen that all three partial derivatives in Eq. (16) go to infinity as the solid fraction, f_s^M, approaches zero. This means that for vanishing solid fractions, very small uncertainties in ρ_l^*, ρ_m, and f_s^M produce a very large uncertainty in the solid density. This is not surprising, since it is difficult to measure solid densities using a mixture that is mostly liquid. Because of the large uncertainties at very low solid fractions, the solid density was only calculated from Eq. (15) for $f_s^M > 5\%$. At $f_s^M = 5\%$, Eq. (16) gives an uncertainty $\delta\rho_s$ of about 4.2×10^{-3} g/cm^3 for all four alloy concentrations. At the highest solid fractions ($<30\%$) for each of the alloy concentrations, the uncertainty $\delta\rho_s$ decreases to about 1.3×10^{-3} g/cm^3. All of these uncertainties in the solid density are large compared to the uncertainty in the measured liquid and liquid–solid mixture densities ($\delta\rho = 1.4 \times 10^{-4}$ g/cm^3), indicating that most of the uncertainty arises from the solid fraction estimates. Nonetheless, the above uncertainties in the solid density, ranging from about 0.1% to 0.4%, can still be considered low for most practical purposes.

3.3.4. Results for the solid density variation

The solid densities during solidification calculated from Eq. (15) for $f_s^M > 5\%$ are plotted in Fig. 7 as a function of temperature for each of the

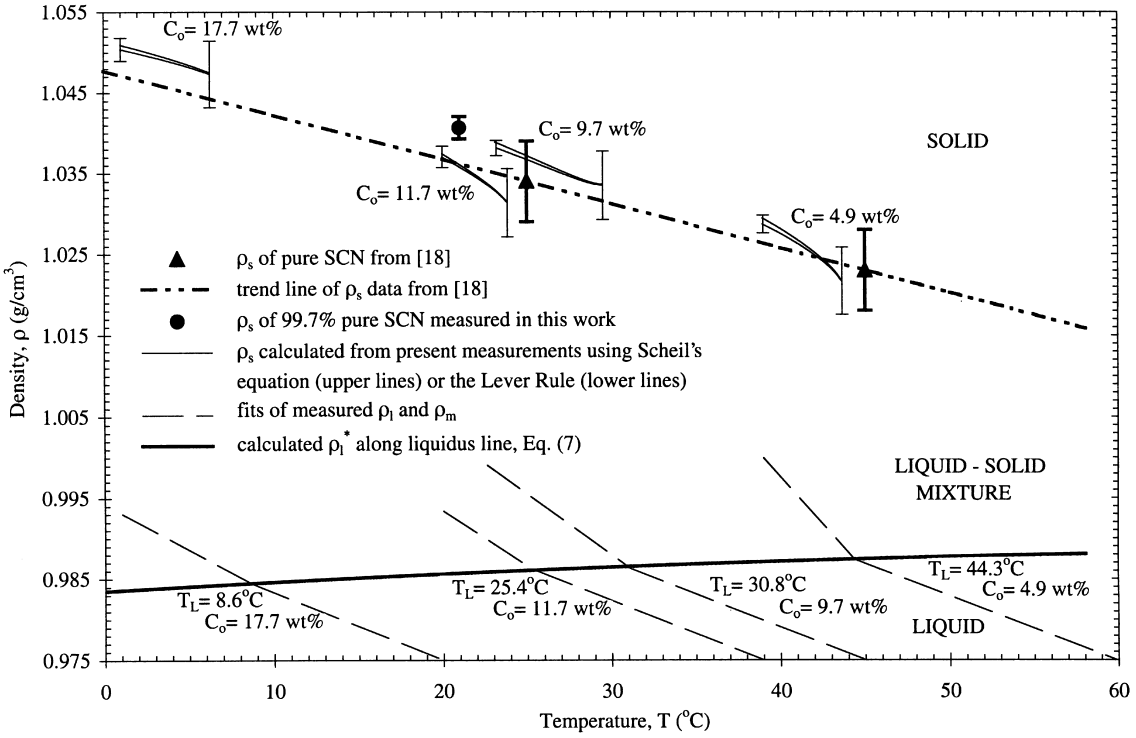

Fig. 7. Solid densities of SCN–ACE during solidification versus temperature for various alloy concentrations, and comparison with solid densities of pure SCN of Wulff and Westrum [18] and of 99.7% pure SCN measured in the present study; for easy reference, liquid and liquid–solid mixture densities are included in the lower portion of the graph.

alloy concentrations C_o. It can be seen that the Lever and Scheil estimates for the solid mass fraction give, as mentioned earlier, similar solid density variations for each C_o. At the highest solid fractions, the difference in the solid densities caused by the two solid fraction estimates is of the same order of magnitude as the total uncertainty in the solid density, $\delta\rho_s$. At lower solid fractions, the two solid fraction estimates give virtually the same solid density, indicating that the consideration of microscopic solute concentration gradients in the solid is not important in analyzing the present measurements.

Also included in Fig. 7 are measured solid densities for pure SCN from Wulff and Westrum [18], together with a trend line through their data assuming a linear variation of the solid density of pure SCN with temperature. It is meaningful to compare the present calculated solid densities to these data for pure SCN, because the low partition ratio, k, of the SCN–ACE system results in very low ACE concentrations in the solid during solidification (at the highest solid fractions, $C_s < 0.6$ wt% for $C_o = 4.9$ wt% and $C_s < 2$ wt% for $C_o = 17.7$ wt%). Fig. 7 shows that the calculated solid densities for the SCN–ACE alloys are generally in the same range as the data of Wulff and Westrum for pure SCN. The addition of ACE can be expected to *decrease* the density of the solid, as is observed for the liquid. The calculated solid densities support this trend. For example at 25°C, the solid density for $C_o = 11.7$ wt% is below that for $C_o = 9.7$ wt%. However, many of the calculated solid densities for the SCN–ACE alloys fall above the trend line for pure SCN in Fig. 7. This apparent contradiction may be explained by the relatively large estimated uncertainty in the density data of Wulff and Westrum [18] (Fig. 7).

Because of the relatively large uncertainty in the Wulff and Westrum [18] data, independent experiments for measuring the solid density of SCN were performed as part of the present study. These experiments are preliminary and limited to room temperature (21°C). More detailed experiments will be reported in a future publication. In brief, condensate was removed from the condenser of a SCN distillery and used to directionally solidify a SCN sample. The purity of the SCN was estimated to exceed 99.7%. The solid density of the SCN sample was measured following the procedure described in an ASTM Standard for determination of glass density by buoyancy [19]. The experiments were repeated several times. The resulting average value of the solid density at 21°C, together with the estimated uncertainty, is plotted in Fig. 7. It can be seen that the present solid density measurement for 99.7% pure SCN falls above the trend line of the pure SCN data of Wulff and Westrum [18], but is still within their uncertainty. More importantly, the data point falls above the solid density estimated for the SCN-11.7 wt% ACE alloy at 21 °C, thus removing any apparent contradiction.

The small range of ACE concentrations in the solid in the present experiments (<2 wt%), and the relatively large uncertainties in the solid densities at low solid fractions, prevent a correlation of the present solid densities as a function of C_s and T [similar to the composite liquid density correlation, Eq. (6)]. Nonetheless, the solid densities presented in Fig. 7 should serve as reasonable estimates for use in a variety of solidification studies.

4. Conclusions

Measurements were made of the liquid and liquid–solid mixture densities of SCN–ACE alloys. The results for the liquid are combined by regression analysis into a correlation that describes the density as a function of temperature and composition, up to about 20 wt% ACE. The composite correlation, Eq. (6), gives the liquid density to within a 95% confidence interval of 1.67×10^{-4} g/cm^3 or about 0.017%. The thermal and solutal expansion coefficients, β_T and $\beta_{C,}$ are then derived from this correlation. In the limit of vanishing ACE concentration, the present results for the liquid density and β_T are found to be in excellent agreement with data available in the literature for pure SCN. This indicates that the trace impurities in the starting SCN have little effect on the present measurements. It is found that the density of the saturated liquid of SCN–ACE alloys is remarkably constant.

Based on density measurements of a finely dispersed liquid–solid mixture (mush), and solid fraction estimates from Scheil's equation or the Lever Rule, solid densities of SCN–ACE alloys during solidification are calculated. An uncertainty analysis reveals that the solid densities are accurate to within about 0.1% to 0.4%, depending on the solid fraction of the mixture. The calculated densities are close to solid densities of pure SCN reported in the literature [18] and of 99.7% pure SCN measured in the present study, which is not surprising since the ACE concentrations in the solid in the alloy experiments are very low. The small ACE concentrations in the solid and the uncertainties in the present solid densities prevent a correlation of the solid density data as a function of concentration and temperature. It is recommended that the solid density of pure SCN be measured over a wider temperature range.

Acknowledgements

The authors gratefully acknowledge the support of this work by NASA under contract NCC8-199 and the help of Dr. Q. Li of the University of Iowa in analyzing the data.

References

[1] M.A. Chopra, Ph.D. Thesis, Rensselaer Polytechnic Institute, 1983.
[2] M.A. Chopra, M.E. Glicksman, N.B. Singh, Metall. Trans. 19A (1988) 3087.
[3] M.E. Glicksman, R.J. Schaeffer, J.D. Ayers, Metall. Trans. 7A (1976) 1747.
[4] J. Lipton, M.E. Glicksman, W. Kurz, Metall. Trans. A 18A (1987) 341.
[5] A. Karma, J.S. Langer, Phys. Rev. A 30 (1984) 3147.
[6] M.A. Eshelman, R. Trivedi, Acta Metall. 35 (1987) 2443.
[7] R. Trivedi, W. Kurz, Int. Mater. Rev. 39 (1994) 49.
[8] S.C. Hardy, Philos. Mag. 35 (1977) 471.
[9] S.C. Huang, Ph.D. Thesis, Rensselaer Polytechnic Institute, 1979.
[10] M. Muschol, D. Lin, H.B. Cummins, Phys. Rev. A 46 (1992) 1038.
[11] ASTM E 542-94, Standard Practice for Calibration of Laboratory Volumetric Apparatus, 1994, p. 301.
[12] R.C. Weast, M.J. Astle, W.H. Beyer, CRC Handbook of Chemistry and Physics, 67th Edition, CRC Press Inc., Boca Raton, FL, 1986.
[13] T. Fang, M.E. Glicksman, S.D. Coriell, G.B. McFadden, R.F. Boisvert, J. Fluid Mech. 151 (1985) 121.
[14] R.F. Brunel, K. Van Bibber, Int. Crit. Tables 3 (1928) 28.
[15] J.W. Brühl, Z. Phys. Chem. 16 (1895) 214.
[16] M.J.F. Eijkman, Rec. Trav. Chim. Pays-Bas. 12 (1893) 274.
[17] J.C. LaCombe, J.L. Oudemool, M.B. Koss, L.T. Bushnell, M.E. Glicksman, J. Crystal Growth 173 (1997) 167.
[18] C.A. Wulff, E.F. Westrum, J. Phys. Chem. 67 (1963) 2376.
[19] ASTM C 693-93, Standard Test Method for Density of Glass by Buoyancy, 1993, p. 212.